

HOSTED BY



Contents lists available at ScienceDirect

Engineering Science and Technology, an International Journal

journal homepage: <http://www.elsevier.com/locate/jestch>

Full length article

Finite element modelling and characterization of friction welding on UNS S31803 duplex stainless steel joints

Mohammed Asif. M, Kulkarni Anup Shrikrishana, P. Sathiya*

Department of Production Engineering, National Institute of Technology, Tiruchirappalli, Tiruchirappalli 620 015, Tamil Nadu, India

ARTICLE INFO

Article history:

Received 17 March 2015

Received in revised form

6 May 2015

Accepted 6 May 2015

Available online xxx

Keywords:

Finite element modelling

Continuous drive friction welding

Duplex stainless steel

Temperature distributions

Axial shortening

ABSTRACT

Solid state joining techniques are increasingly employed in joining duplex stainless steel materials due to their high integrity. Continuous drive friction welding is a solid state welding technique which is used to join similar and dissimilar materials. This joining technique is characterized by short cycle time, low heat input and narrow heat affected zones. The simulation becomes an important tool in friction welding because of short welding cycle. In the present work, a three dimensional non-linear finite element model was developed. The thermal history and axial shortening profiles were predicted using ANSYS, a software tool. This numerical model was validated using experimental results. The results show that the frictional heating stage of the process has more influence on temperature and upsetting stage has more impact on axial shortening. The knowledge of these parameters would lead to optimization of input parameters and improvement of design and machine tools.

Copyright © 2015, The Authors. Production and hosting by Elsevier B.V. on behalf of Karabuk University. This is an open access article under the CC BY-NC-ND license (<http://creativecommons.org/licenses/by-nc-nd/4.0/>).

1. Introduction

Duplex stainless steel belongs to a family of steel with high corrosion resistance than austenitic stainless steels and better weldability than ferritic stainless steels [1]. It is characterised by its unique ferritic/austenitic microstructure. DSS has a wide range of applications in chemical industry, offshore industry, in nuclear reactors and as a structural material [1,2]. Continuous drive friction welding is one of the most popular and often used solid state welding processes. In this type, the materials are joined by heat generation at the faying surfaces and by application of pressure. The heat is generated by conversion of mechanical energy into thermal energy at the joint interface due to rotation under pressure. Friction welding involves thermo-mechanical working those results in grain refinement of the weld zone [3]. This welding method is characterised by low heat input, material save and an easy application. Friction welding can be used for joining various shapes like rod to rod, rod to plate, etc. [4].

The friction welding cycle consists of two stages-heating stage and upsetting stage. In the heating stage, the faying surfaces are

kept in contact and one of the parts is rotated and pressure is applied on the non-rotating part. This pressure is known as 'heating pressure'. The time for which this pressure is applied is 'heating time'. The parts get heated up due to friction between faying surfaces. In the upsetting stage, the rotation is stopped by braking and the pressure is increased. In this stage, due to higher pressure the forging of parts takes place. This pressure is taken as 'upsetting pressure'. The time for which it is applied is given as 'upsetting time'. Axial shortening is reduction in length of the work pieces due to thermo-mechanical working. The joining of duplex stainless steel is a complex process though the material shows good weldability. The fusion welding techniques generally result in unbalanced ferrite-austenite ratios due to melting and solidification [1,2]. This results in deterioration of impact toughness and corrosion resistance of the weldments. Also there is a possibility of formation of secondary phases. Hence solid state joining methods are increasingly becoming popular to join various duplex stainless steel grades. Considering the advantages of continuous drive friction welding, it has drawn the attention of lot of researchers over the last few decades to join similar and dissimilar materials [5]. Many studies have been conducted to develop a numerical model of continuous drive friction welding of various materials.

Sahin [6] developed a computer program using Visual Basic software. The simulation of continuous drive friction welding of two concentric cylindrical rods was carried out using subroutines.

* Corresponding author. Tel.: +91 4312503510; fax: +91 4312500133.

E-mail address: psathiya@nitt.edu (P. Sathiya).

Peer review under responsibility of Karabuk University.

He used finite difference method to predict material deformations i.e. flash formations as well as temperature at weld interface. Kahveci et al. [7] formed governing equations to solve heat transfer problem in continuous drive friction welding. The cylindrical rods of different shapes and materials were considered in the problem. The radial and axial temperature distributions and thermal gradients were determined successfully using a numerical model. Qinghua et al. [8] carried out FEM simulation of friction welding of Al–Cu–Mg alloy. The various parameters studied were thermal distribution, stresses and strains at the interface of the two rods. A two dimensional coupled thermo-mechanical model was established with axisymmetric geometry. The simulations were carried out using MSC. Marc software. They found that 2D FE model resulted in a considerable error between experimental and simulated values. Seli et al. [9] used explicit one dimensional FE model to study friction welding of aluminium and mild steel. They studied the temperature distribution by considering both heating and cooling stage of welding. The effects of flash formation were neglected in the model. The thermal effects of welding on hardness were also studied. The simulated data showed a fair agreement with the experimental results. Li and Wang [10] simulated the continuous drive friction welding of mild steel using ABAQUS software. The influence of axial pressure and speed of rotation on temperature field and axial shortening were determined. Shu-de et al. [11] studied 3D numerical model of material flow behaviour of friction welded 45[#] steel. They used DEFORM 3D software to study the influence of friction pressure, friction time and rotational velocity on flash formation. The tetragonal four node element was used to mesh the component. Recently, Hynes et al. [12] carried out simulation of heat flow in friction welding of dissimilar materials. They used ANSYS software tool with 8 node 45 brick type mesh element. Though the effect of flash formation was not considered, the numerical results show a good agreement with experimental data.

From the above literature review it can be confirmed that there is lack of studies on the continuous drive friction welding of duplex stainless steel. It was also proved that 3D models were more reliable than 2D models of continuous drive friction welding [13]. From the literature review, it is clear that there has not been a detailed study on FE modelling friction welding of duplex stainless steel. In the present work, a 3D FEM model has been developed to study temperature distribution and axial shortening during friction welding by considering the effects of conduction, radiation and convection. Also an experimental setup was made to join two similar duplex stainless steel cylindrical rods to validate the simulation results. The scientific goals of this work are to predict thermal history and axial shortening during friction welding with

Table 1
Chemical composition of base material.

Element	C	N	Mn	S	Cr	Mo	Ni	Cu	Fe
% wt	0.02	0.14	1.60	0.01	21.65	2.56	4.84	0.43	Balance

Table 2
Material properties of base material.

Property	Range
Density	7805 kg/m ³
Melting point range	1390–1443 °C
Thermal conductivity	16–22 W/m-K
Specific heat capacity	469 J/Kg-K
Poisson's ratio	0.33

the help of commercial engineering analysis software and also to understand thermo-mechanical effects on weld properties.

2. Materials and methods

2.1. Material

In this investigation, UNS S31803 Duplex stainless steel rods of diameter 16 mm were used. These were cut into 100 mm length each. The chemical composition of the material was tested based on ASTM E1086 standards and the related data are given in Table 1.

As received material properties are listed in Table 2.

The variation of flow stress and Young's modulus with temperature are shown in Fig. 1.

2.2. Friction welding experiments

The welding experiments were carried out on the basis of Taguchi design of experiments procedure. In this study, four parameters were selected at three levels. The process parameters and their respective levels are given in the Table 3.

In taguchi, each parameter will yield two degrees of freedom and total eight degrees of freedom for all four parameters. Therefore the experimental array should have minimum eight degrees of freedom i.e. minimum nine experiments. Hence, nine different sets of process parameters were formed to form a L9 orthogonal array which is shown in Table 4.

Welding experiments were done on KUKA friction welding machine with a constant rotational speed of 1500 rpm given to each of the work pieces during the frictional heating stage. The

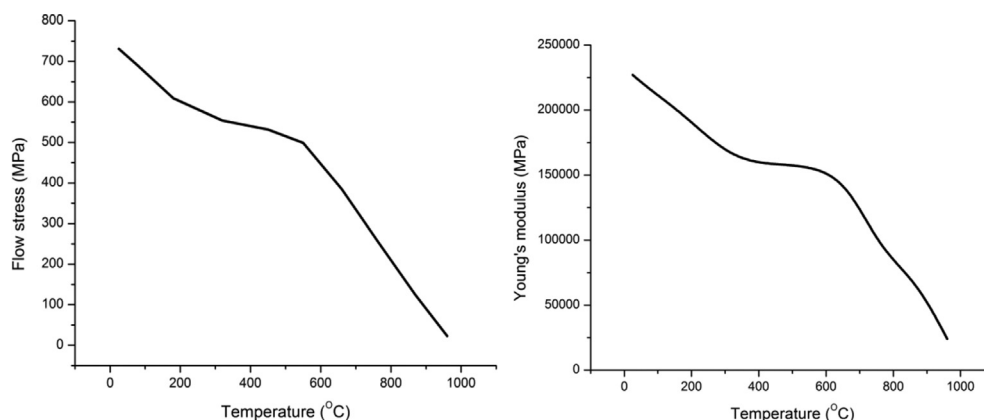


Fig. 1. The variation of flow stress and Young's modulus with temperature [14].

Table 3
Welding parameter and their levels.

Sr. No.	Parameters	Level 1	Level 2	Level 3
1	Heating pressure (MPa)	30	40	50
2	Heating time (sec)	3	4	5
3	Upsetting pressure (MPa)	60	70	80
4	Upsetting time (sec)	2	3	4

Table 4
L9 Orthogonal array based experimental parameters layout.

Experiment no.	Heating pressure (MPa)	Heating time (sec)	Upsetting pressure (MPa)	Upsetting time (sec)
1.	30	3	60	2
2.	30	4	70	3
3.	30	5	80	4
4.	40	3	70	4
5.	40	4	80	2
6.	40	5	60	3
7.	50	3	80	3
8.	50	4	60	4
9.	50	5	70	2

experimental set-up is shown in Fig. 2. Welded joints that were produced using each set of parameters are shown in Fig. 3.

It can be seen from Fig. 3, that joints were obtained successfully, and flash formation was observed in all cases. The axial shortening was measured and it was found to be varying in each case.

2.3. Testing and measurements

After the welds were successfully completed, the flash was removed by machining. The samples were cut and the surface of the weld were polished up 1200 grit fineness and cloth polished through 0.05 μm grain size alumina powder and finally etched for analysing weld microstructures. On transverse track of the weld path, microhardness measurement was taken all around which covers parent material, PDZ and weld metal. Vickers microhardness tester was used with indentation load of 500 g, dwell time of 15 s and indentation speed of 50 $\mu\text{m/s}$. Experimental temperature measurements throughout the friction welding were measured through a non – contact infrared thermometer control using a computer data logger. The XRD analysis was done through Rigaku Ultimate X-ray diffractometer with CuK α radiation of wavelength 1.544 \AA .

3. Mathematical modelling

The friction welding process follows the classical Coulomb's friction law which relates shear stress at contact and axial pressure [15]:

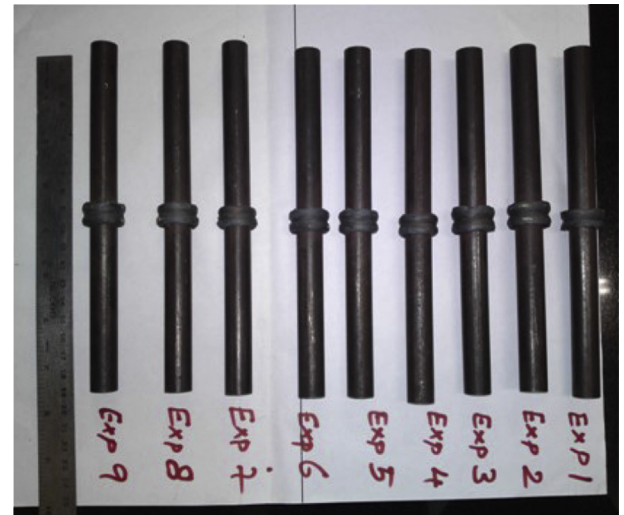


Fig. 3. Weld joints of various parameters.

$$\tau_f = \mu P \quad (1)$$

where, τ_f is the shear stress induced, μ is the coefficient of friction and P is the axial pressure.

At lower temperatures classical coulomb's law is valid but at higher temperatures visco-plastic friction is dominant at the interfaces. Hence equivalent flow stress is given by modified Coulomb's law [15]:

$$\tau_{shear} = \tau_f = \frac{\sigma_s}{\sqrt{3}} \quad (2)$$

where τ_{shear} is the flow shear stress and σ_s is the equivalent flow stress.

Hence heat generation during friction welding is given by [14]:

$$Q = \eta * \gamma * \tau_f = \eta * \gamma * \min \left(\mu P, \frac{\sigma_s}{\sqrt{3}} \right) \quad (3)$$

where γ is the slipping rate and η is the heat efficiency. In most of the cases heat generation in visco-plastic friction condition is considered.

Some authors considered heat generation in two parts: Heat generation during plastic deformation as given by Equation (3) and heat generation at the interface due to sliding friction which is given by [10,15]:

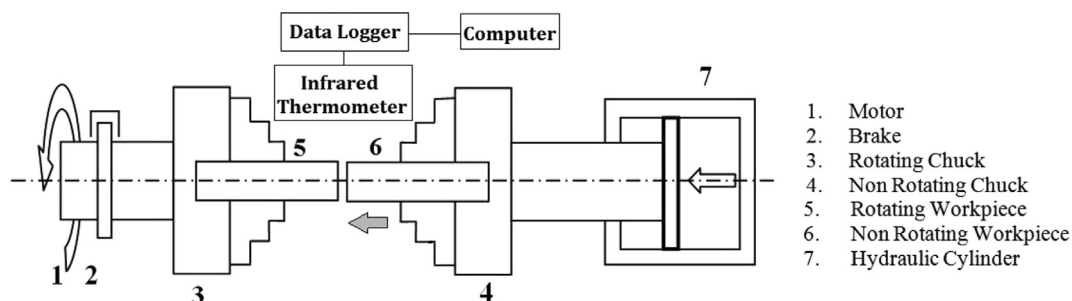


Fig. 2. Experimental setup of continuous drive friction welding.

$$Q = \delta * \eta * \gamma * \mu * P + (1 - \delta) * \eta * \gamma * \left[\frac{\sigma_s}{\sqrt{3}} \right] \quad (4)$$

where δ is fraction related to sliding friction.

The equation for thermal modelling of this problem is given by Fourier heat conduction phenomenon which is written as [12]–

$$k \left[\frac{\partial^2 T}{\partial x^2} + \frac{\partial^2 T}{\partial y^2} + \frac{\partial^2 T}{\partial z^2} \right] + Q = \rho C_p \frac{\partial T}{\partial t} \quad (5)$$

where T is the temperature, Q is heat generation rate, t is time, k is thermal conductivity, C_p is the specific heat capacity and ρ is the materials density. Q and T are functions of x , y , z and t .

4. FEM of continuous drive friction welding

The simulation of continuous drive friction welding was performed using ANSYS software. The objective of this study is to simulate thermal effects and axial shortening during welding cycle. The material properties given to the model are as in Table 2. The temperature dependent material properties were fed to the software. A coupled thermo-mechanical transient analysis was chosen for the simulation.

4.1. Geometry and meshing

A three dimensional model consisting of two parts was created in ANSYS which was dimensionally similar to the two work pieces of diameter 16 mm and length 100 mm each. Since it was intended to perform simulation taking the thermal and mechanical effects simultaneously into consideration, selecting the suitable element type to mesh the model was particularly important. ANSYS provides a three dimensional meshing with tetrahedron shaped element. This element has the capability to perform coupled thermo-structural analysis. The accuracy of finite element model always depends on meshing. Initially, the computations were done with coarser meshing. Though the solution was converged, the results obtained were not in the acceptable tolerance of experimental results. Later the mesh refinement was done until the solution was independent of mesh refinements and the solution could be within the range of acceptance. This mesh was considered to be the best one and it was selected for the simulations. Finally, the total numbers of nodes were 7043 and the elements were 27147. This welding technique is characterized by narrow heat affected zone hence a fine meshing was employed in a small region near the weld interface. A coarse meshing was used for the rest of

the geometry to save the computation time. To model the frictional contact between the rods, the contact surfaces were meshed using special purpose element types like conta174 and targe170, thus forming a frictional contact pair. The complete geometry and meshing are shown in Fig. 4.

4.2. General assumptions

For analysis of continuous drive friction welding, the heat generated and pressure across the weld interface were assumed to be uniform. In reality the heat distribution varies along the radial distance from the centreline of the component. But to avoid complexity this assumption was made. The duplex stainless steel material was assumed to be homogeneous and isotropic. The end parts of the component which hold the part i.e. chucks were not considered in this model.

4.3. Boundary conditions

In friction welding, nodes on the surface of non-rotating component parallel to friction surface are completely constrained. The loading i.e. pressure was applied on surfaces of rotating component which were parallel to friction surfaces, with direction of pressure being perpendicular to friction surface. The loading was given in two steps similar to actual process. It is assumed that parts are initially in contact.

In thermal boundary conditions, the heat loss due to convection, conduction and radiation were considered. Heat generation was given at weld interface which was calculated by equation no. 4. In heat losses, the material emissivity was taken as 0.4 and the heat transfer coefficient was taken as 25 W/m²-K throughout the analysis. The detailed boundary conditions can be seen in Fig. 5.

4.4. Material model

The Johnson–Cook damage model was considered. The flow stress (σ) is a function of strain hardening, strain rate hardening and temperature softening as given in the following equation:

$$\sigma = (A + B\varepsilon^n) * \left[1 + C \ln \left(1 + \frac{\dot{\varepsilon}}{\dot{\varepsilon}_0} \right) \right] * \left[1 - \left(\frac{T - T_{room}}{T_{melt} - T_{room}} \right)^m \right] \quad (6)$$

The first, second and third brackets of Equation (6) represent elastic–plastic, viscosity and thermal softening terms of Johnson–Cook model. Here ε , $\dot{\varepsilon}$ and $\dot{\varepsilon}_0$ are strain, strain rate and reference strain rate respectively. T_{room} and T_{melt} are room temperature and melting temperature respectively. A , B , C , n and m are material

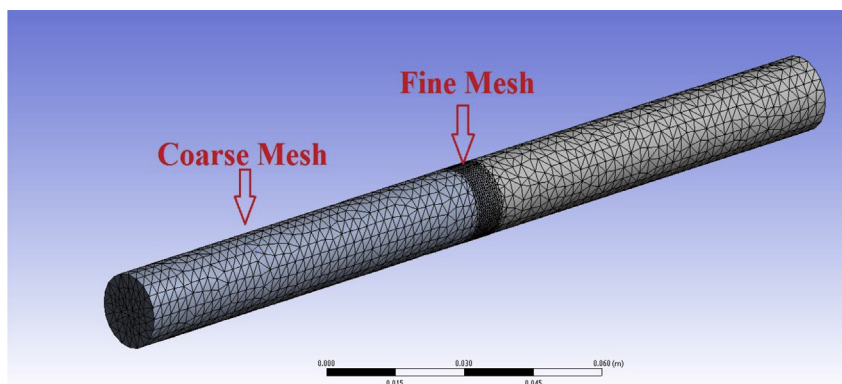


Fig. 4. Complete geometry and meshing.

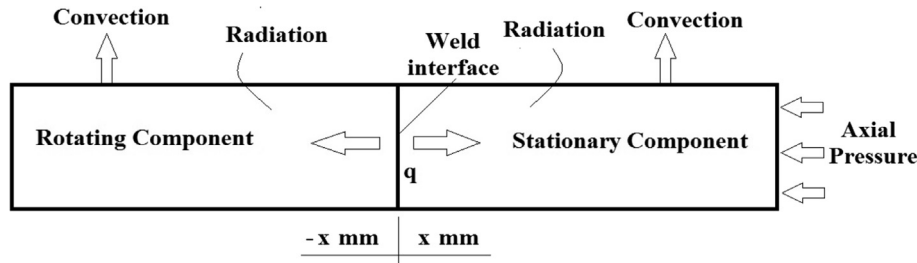


Fig. 5. Boundary conditions.

Table 5

Parameters for Johnson–Cook model.

A (MPa)	B (MPa)	C	n	m	$\dot{\epsilon}_0$ (m/s)
731	840.50	0.0124	0.1904	0.965	1

dependent constants. The values of the parameters of the Johnson–Cook damage model are given in Table 5.

The material constants in Johnson–Cook model were calculated by following procedure- [16].

- The value of A was the yield stress of the material taken from Fig. 1
- Then the curve $\ln(\sigma - A)$ vs $\ln(\dot{\epsilon})$ was plotted by assuming $T = T_{\text{room}}$ and $\dot{\epsilon} = \dot{\epsilon}_0$. The value B and n were the intercept and the slope of $\ln(\sigma - A)$ vs $\ln(\dot{\epsilon})$ curve respectively.
- The values of A, B, n were substituted in Equation (6) It was assumed that $T = T_{\text{room}}$, which eliminated the thermal softening term. Then the strain rate coefficient (C) was obtained from the slope of the graph $\ln\left(\frac{\sigma}{A+B\dot{\epsilon}^n}\right)$ vs $\ln(\dot{\epsilon})$.
- The viscosity term was eliminated by assuming $\dot{\epsilon} = \dot{\epsilon}_0$, the exponent m was obtained from slope of the graph $\ln\left(1 - \left[\frac{\sigma}{A+B\dot{\epsilon}^n}\right]\right)$ vs $\ln\left(\frac{T - T_{\text{room}}}{T_{\text{melt}} - T_{\text{room}}}\right)$.

ANSYS provides an option to include the temperature dependent material properties and also the material model that can be included by feeding the Johnson–Cook model parameters to the software.

4.5. Simulation

The transient analysis was performed to simulate the friction welding problem. The presence of frictional contact and deformed geometry made the analysis non-linear in nature. The loading was given in two load steps, similar to the two stages in the actual process, although it was assumed that initially the parts to be welded were in contact. The load steps were according to the respective heating time and upsetting time parameters. The effects of cooling after the end of second load step were considered in the simulation. Automatic time stepping feature in ANSYS was utilised for reducing the simulation time.

Table 6

Simulated and experimental peak temperatures.

Exp. No.	1	2	3	4	5	6	7	8	9
Simulated Peak temperature (°C)	812.62	934.01	953.45	897.23	970.21	970.47	964.62	950.54	983.54
Experimental Peak temperatures (°C)	770.50	880.70	927.60	847.40	937.10	929.40	920.90	905.30	930.30

5. Results and discussion

In the present study, simulation of continuous drive friction welding of duplex stainless steel was carried out. Experiments were carried out to validate the results of numerical simulation.

5.1. Nodal temperature

The temperature distribution was determined using an infrared thermometer. The temperatures were measured at the weld interfacial region and along the length of the component. Simulated and experimental peak temperatures were shown in Table 6.

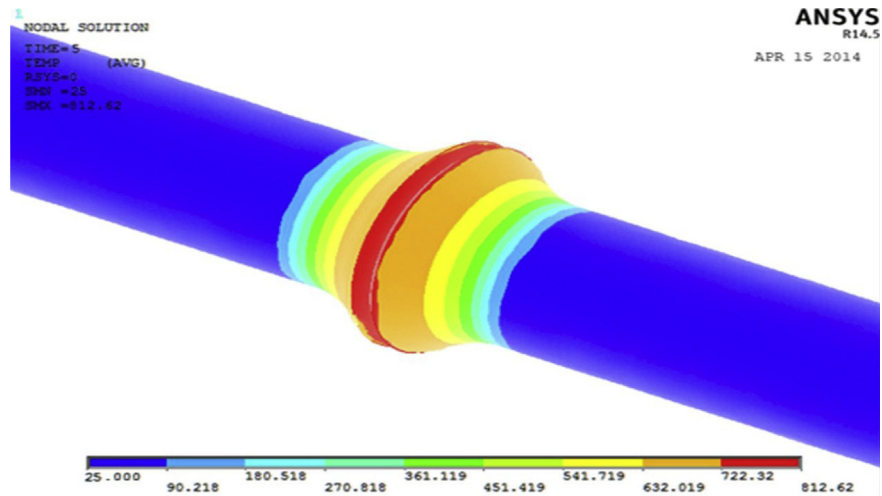
From Table 6, it is clear that the peak temperatures obtained are much below the melting point temperature of the material. The simulated peak temperatures were in agreement with the experimental peak temperatures. The difference between the experimental and simulated results could be attributed to the complex nature and the assumptions made during the process. The uniform application of pressure on the faying surface and omission of the effect of cooling could be the reasons to cause an error. In overall, the accuracy of 95% has been achieved with this model. Increase in temperatures gave higher hardness values along the weld interface and this was due to grain refinement that took place by plastic deformation and high cooling rate. The thermal effects are prominent only near the weld interface. The simulated thermal distribution of experiment no. 1 and 9 are shown in Fig. 6.

From Fig. 6(a) and (b), it can be seen that, final temperature is very high near the weld interface and the gradient of the temperature is very steep in the axial direction. Visually axial shortening is also very less as compared to experiment no. 9 which has a fair agreement with actual experiment, as shown in Fig. 8. The length vs temperature graph is shown in Fig. 7, in which the origin of the abscissa $x = 0$ represents the weld interface. The graph is shown for experiment no. 1 and experiment no. 9.

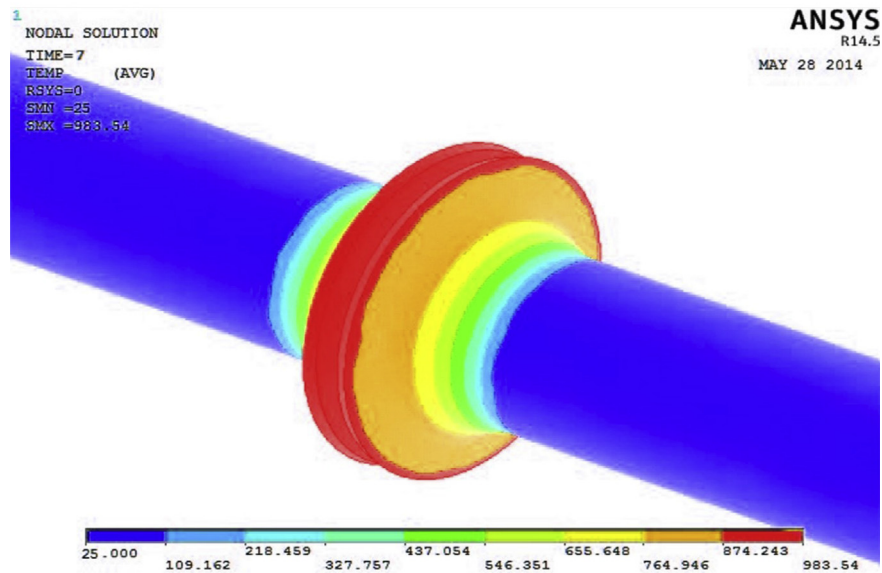
Fig. 7 shows that the temperature decreases gradually from the peak value to either side of the weld interface. The temperature profile is symmetric about weld interface due to similar material welding. It can be seen that the temperature rise in heating stage is very high as compared to upsetting stage. This is due to low heat generation during the upsetting stage.

5.2. Axial shortening

Axial shortening is defined as the loss in length of the material of the component at the end of the friction welding process. ANSYS



(a) Simulated thermal distribution of Experiment 1



(b) Simulated thermal distribution of Experiment 9

Fig. 6. Simulated thermal distribution of various experiments.

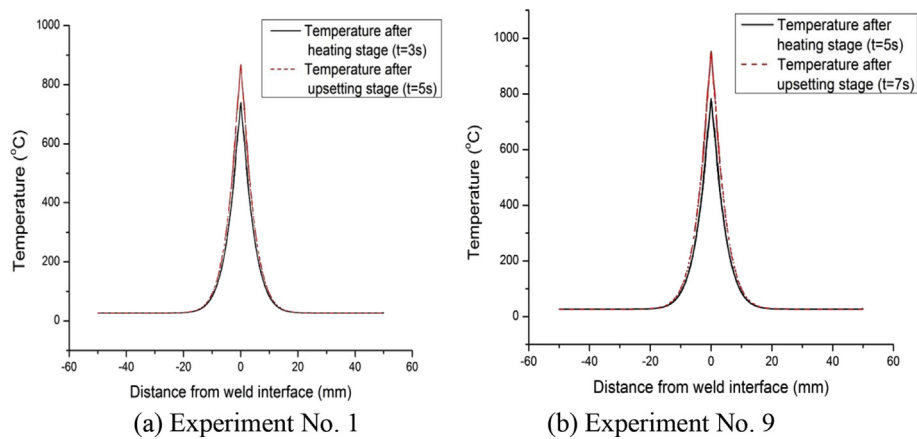


Fig. 7. Temperature distributions along the component axis.

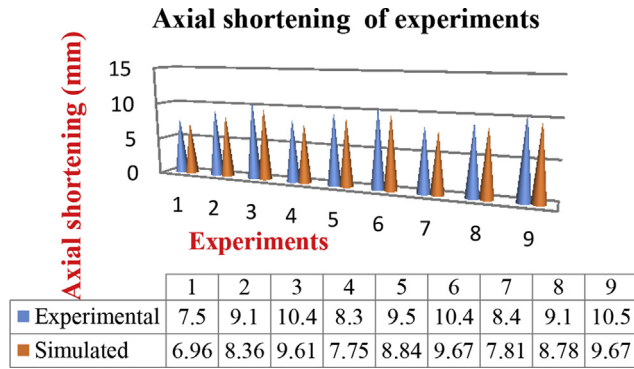


Fig. 8. Comparison of simulated axial shortening values with actual experimental results.

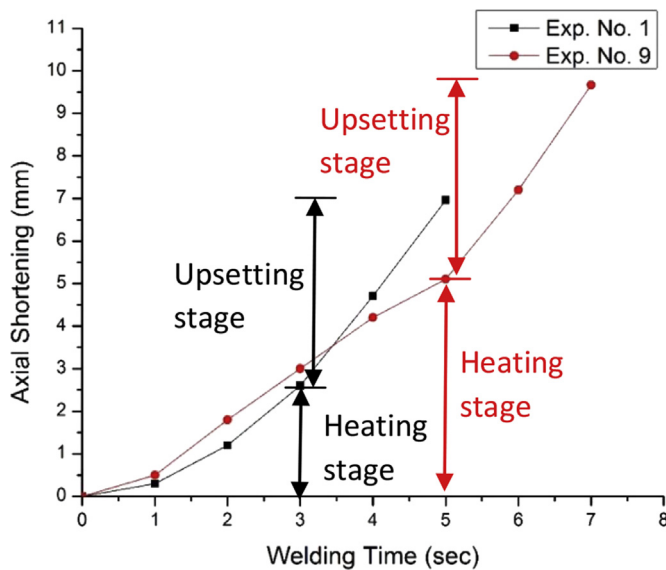


Fig. 9. Axial shortening vs welding time.

provides the deformation calculations at the end of the process. These deformations in the two bodies were combined and the value was taken as axial shortening. Flash formation was observed in all of the samples and varied values of axial shortenings were obtained

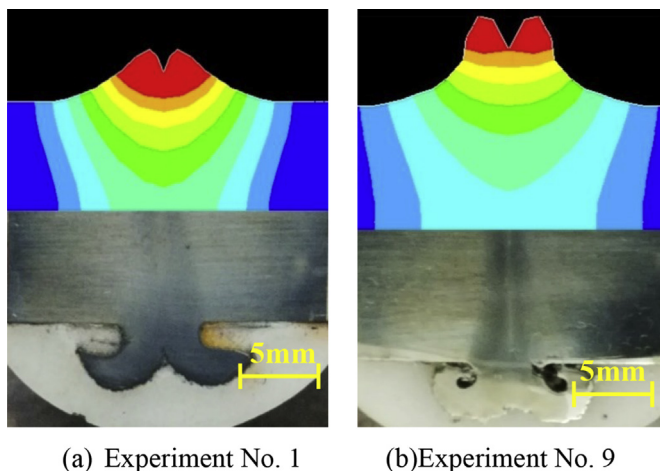


Fig. 10. Flash shape of the model compared with the actual experiment.

in each case. Fig. 8 shows variation of simulated axial shortening with actual experimental shortening values.

It is clear from Fig. 8, that when the simulated results are compared to the experimental results, they differed by a maximum error of about 8% which shows the feasibility of developed finite element model. The variation of axial shortening with welding time is given in Fig. 9.

From Fig. 9, It can be observed that axial shortening is not appreciable until first few seconds of heating stage. After that, flash begins to form and there is a considerable axial shortening at the end of heating stage. But the flash increases sharply in upsetting stage for all the experiments. This can be attributed to the fact that the high temperature thermoplastic material is forged during upsetting giving high strain values. Similar observations were made in previous studies [10]. Fig. 10 shows the similarity between final cross-sectional flash shape of the model and the actual experimental specimens 1 and 9 as shown in Fig. 10(a) and (b) respectively.

From Fig. 10, a good agreement could also be found between the flash shapes of the model and the experiment. It is possible to predict the shape of the flash with a high degree of accuracy. Therefore, the developed model in this study can be used to simulate the friction welding process. An error was observed in the shape of the flash which was due to complex nature and the assumptions made during the weld process.

5.3. Metallography

Microstructural studies of weldments revealed three distinct zones namely-weld zone (WM), partially deformed zone (PDZ) and base material (BM). The macrograph and micrograph of weld sample is shown in Fig. 11.

From Fig. 11, it can be observed that all the weldments showed unique grain orientations. The size of the three different zones was dependent on the upset pressure in the welding. The weld region is characterized by very fine grains which occur due to dynamic recrystallization in the region. The partially deformed zone is the heat affected zone where slightly less deformation occurs as compared to the weld region. The most of the component remain unaffected which gives the microstructure of base material.

Fig. 12 shows the SEM images of weld region and PDZ for experiment no. 9. It can be seen that austenite has been formed in ferrite matrix.

The XRD patterns were plotted for the experiments. The Fig. 13 shows XRD plot for experiments no. 1, 9 and base material.

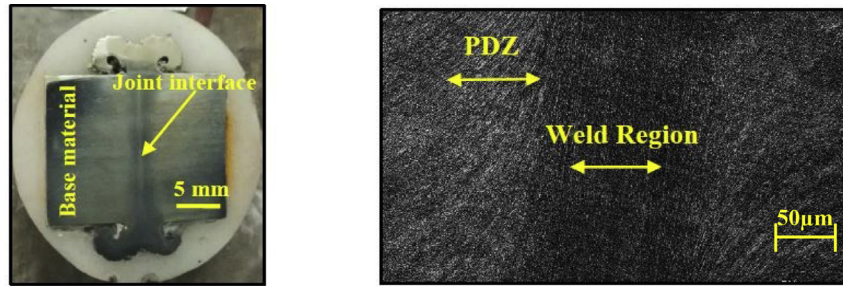
From Fig. 13, it was found that there is no difference between XRD patterns of base material and welded samples besides some variation in peak intensities. Hence it can be proved that no undesired intermetallic phases were formed after welding.

5.4. Microhardness

To study the variation in hardness in regions of base metal (B.M.), partially deformed zone (PDZ) and weld metal (WM), microhardness test was conducted successfully. The joint results are provided in Table 7.

The Fig. 14 shows distribution of hardness around the weld sample for various experiments.

From Fig. 14, it is clear that the hardness for the welded materials is higher near the interface when compared to PDZ. This is due to the strain hardening effect during the friction process at the interface [17]. The hardness of the heat affected zones were found to be lower than the base material in all the experiments. This is due to dominant thermal effect at the weld interface compared to worked effect [9].



(a) Macrograph of weld (sectional view)

(b) Micrograph of weldments (Exp. No. 9)

Fig. 11. Macrograph and micrograph of weld interface.

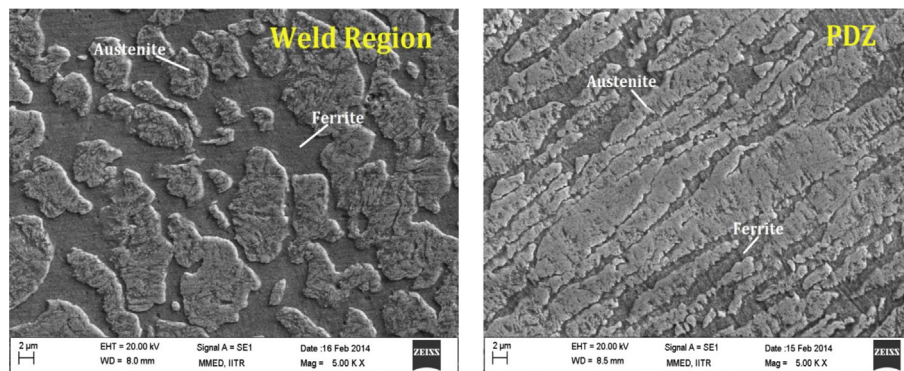


Fig. 12. SEM images of weld and PDZ.

Table 7
Microhardness values of friction welded.

Exp. No.	1	2	3	4	5	6	7	8	9
Parent metal (Hv)	294	316	310	322	278	327	361	312	326
WM (Hv)	284	281	288	303	292	303	304	306	298
PDZ (Hv)	278	280	283	284	284	289	284	290	290

6. Conclusion

Continuous drive friction welding of duplex stainless steel was simulated using 3D non-linear finite element model developed in ANSYS. The thermal history and axial shortening were studied

using experimental and numerical results. The following conclusions were drawn from the study.

1. The simulation results of temperature distributions, peak temperatures and axial shortening showed a fair agreement with actual experimental results.
2. Online temperature measurement was done using infrared thermometer. It was found that the highest temperature rise occurred during frictional heating stage. The peak temperatures are much below the melting point of the material. A large amount of axial shortening is obtained in the upsetting stage as compared to heating stage due to high temperature forging of the material.

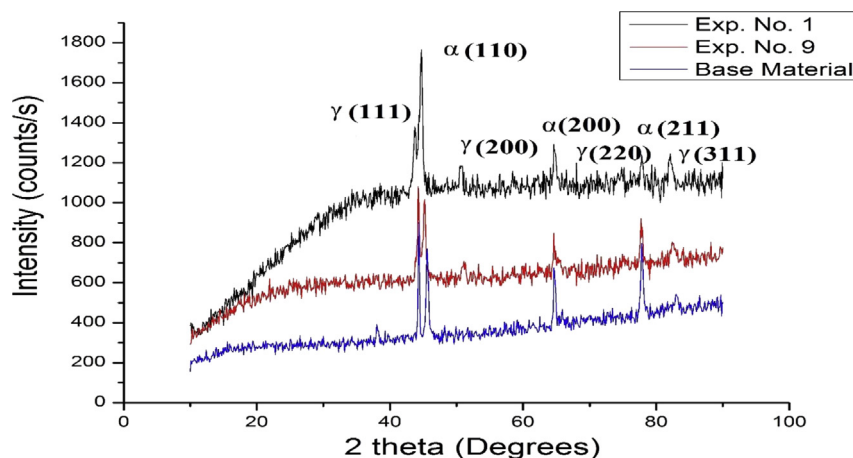


Fig. 13. XRD plot of various experiments.

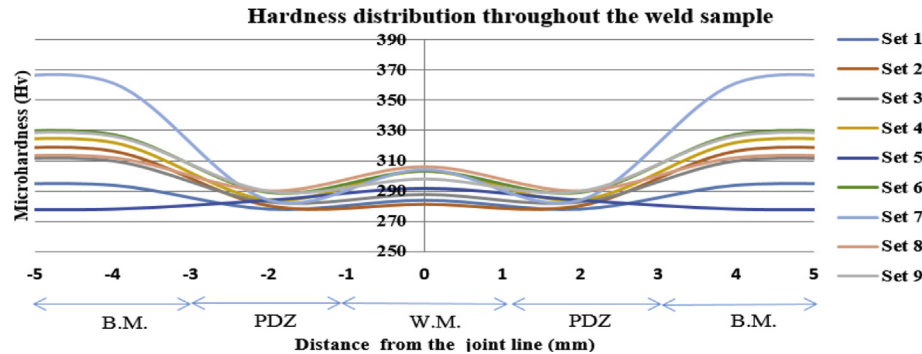


Fig. 14. Distribution of microhardness in friction welded samples.

3. From the metallurgical characterization, it is confirmed that no intermetallic phases are formed after welding. The thermal effects are dominant as compared to mechanical worked effect. This was confirmed from the hardness measurements.

Acknowledgement

We would like to express our deepest appreciation and sincere thanks to Council of Scientific and Industrial Research (CSIR), New Delhi, India, for financially supporting this entire research work, under the scheme of sponsored research project sanctioned No. 22 (0596)/12/EMR-II dated 02.04.2012.

References

- [1] Y.S. Sato, T.W. Nelson, C.J. Sterling, R.J. Steel, C.-O. Pettersson, Microstructure and mechanical properties of friction stir welded SAF 2507 super duplex stainless steel, *Mater. Sci. Eng. A* 397 (2005) 376–384, <http://dx.doi.org/10.1016/j.msea.2005.02.054>.
- [2] K.W. Chan, S.C. Tjong, Effect of secondary phase precipitation on the corrosion behavior of duplex stainless steels, *Mater. (Basel)* 7 (2014) 5268–5304, <http://dx.doi.org/10.3390/ma7075268>.
- [3] G.S. Chander, G.M. Reddy, A.V. Rao, Influence of rotational speed on microstructure and mechanical properties of dissimilar metal AISI 304–AISI 4140 continuous drive friction welds, *J. Iron Steel Res. Int.* 19 (2012) 64–73.
- [4] M. Sahin, H.E. Akata, T. Gulmez, Characterization of mechanical properties in AISI 1040 parts welded by friction welding, *Mater. Charact.* 58 (2007) 1033–1038, <http://dx.doi.org/10.1016/j.matchar.2006.09.008>.
- [5] N. Rajesh Jesudoss Hynes, P. Nagaraj, J. Angela Jenniffa Sujana, Mechanical evaluation and microstructure of friction stud welded aluminium–mild steel joints, *Arab. J. Sci. Eng.* 39 (2014) 5017–5023, <http://dx.doi.org/10.1007/s13369-014-1082-y>.
- [6] M. Sahin, Simulation of friction welding using a developed computer program, *J. Mater. Process. Technol.* 153–154 (2004) 1011–1018, <http://dx.doi.org/10.1016/j.jmatprotec.2004.04.287>.
- [7] K. Kahveci, Y. Can, A. Cihan, Heat transfer in continuous-drive friction welding of different diameters, *Numer. Heat Transf. Part A Appl. An Int. J. Comput. Methodol.* 48 (2005) 1035–1050, <http://dx.doi.org/10.1080/10407780500283291>.
- [8] L. Qinghua, L. Fuguo, L. Miaoquan, W. Qiong, F. Li, Finite element simulation of deformation behavior in friction welding of Al–Cu–Mg alloy, *J. Mater. Eng. Perform.* 15 (2006) 627–631, <http://dx.doi.org/10.1361/105994906X150821>.
- [9] H. Seli, A.I.M. Ismail, E. Rachman, Z.A. Ahmad, Mechanical evaluation and thermal modelling of friction welding of mild steel and aluminium, *J. Mater. Process. Technol.* 210 (2010) 1209–1216, <http://dx.doi.org/10.1016/j.jmatprotec.2010.03.007>.
- [10] W. Li, F. Wang, Modeling of continuous drive friction welding of mild steel, *Mater. Sci. Eng. A* 528 (2011) 5921–5926, <http://dx.doi.org/10.1016/j.msea.2011.04.001>.
- [11] S. Ji, J. Liu, Y. Yue, Z. Lü, L. Fu, 3D numerical analysis of material flow behavior and flash formation of 45# steel in continuous drive friction welding, *Trans. Nonferrous Met. Soc. China* 22 (2012) s528–s533, [http://dx.doi.org/10.1016/S1003-6326\(12\)61756-7](http://dx.doi.org/10.1016/S1003-6326(12)61756-7).
- [12] N. Rajesh Jesudoss Hynes, P. Nagaraj, R. Palanichamy, C.A.K. Arumugham, J. Angela Jenniffa Sujana, Numerical simulation of heat flow in friction stud welding of dissimilar metals, *Arab. J. Sci. Eng.* 39 (2014) 3217–3224, <http://dx.doi.org/10.1007/s13369-013-0932-3>.
- [13] Q.Z. Zhang, L.W. Zhang, W.W. Liu, X. Zhang, W. Zhu, Shen QU, Comparison of 3D and 2D numerical simulation of continuous-drive friction welding process, *Trans. Weld. Inst.* 27 (2006) 105.
- [14] J. Chen, B. Young, Stress–strain curves for stainless steel at elevated temperatures, *Eng. Struct.* 28 (2006) 229–239, <http://dx.doi.org/10.1016/j.engstruct.2005.07.005>.
- [15] W. Li, S. Shi, F. Wang, Z. Zhang, T. Ma, J. Li, Numerical simulation of friction welding processes based on ABAQUS environment, *J. Eng. Sci. Technol. Rev.* 5 (2012) 10–19.
- [16] R.D. Koyee, S. Schmauder, U. Heisel, R. Eisseler, Numerical modeling and optimization of machining duplex stainless steels, *Prod. Manuf. Res. An Open Access J.* 3 (2015) 36–83, <http://dx.doi.org/10.1080/21693277.2014.990539>.
- [17] A.V. Jebaraj, L. Ajaykumar, Influence of microstructural changes on impact toughness of weldment and base metal of duplex stainless steel AISI 2205 for low temperature applications, *Proc. Eng.* 64 (2013) 456–466, <http://dx.doi.org/10.1016/j.proeng.2013.09.119>.